

Electronic pseudogap of optimally doped $\text{Nd}_{2-x}\text{Ce}_x\text{CuO}_4$

D. K. Sunko* and S. Barjšić†

Department of Physics, Faculty of Science, University of Zagreb,
Bijenička cesta 32, HR-10000 Zagreb, Croatia.

We study the effect of antiferromagnetic correlations in the three-band Emery model, in comparison with the experimental angle-resolved photoemission (ARPES) spectra in optimally doped NCCO. The same calculation, formerly used to describe BSCCO, is applied here, but in contrast to BSCCO, where quantum paramagnon fluctuations are important, the characteristic energy of the dispersive paramagnons in NCCO is of the order of T_c . The wide dispersing features of the single-electron spectrum in NCCO are analogous to the BSCCO hump. The Fermi surface is pseudogapped in both the nodal and antinodal directions, although the detailed features differ, being dominated by loss of intensity in the nodal direction, and loss of coherence in the antinodal one. Direct oxygen-oxygen hopping is important in NCCO as well as in BSCCO, in order to obtain overall agreement with the measured ARPES spectra.

PACS numbers: 74.25.Jb, 74.72-h, 79.60-i

High-temperature superconductivity (SC) is one of the premier problems of physics today. It occurs across a broad range of copper oxide perovskites, whose electronic responses are quite dissimilar. The *n*-doped high-temperature superconductors show a number of outstanding differences with the *p*-doped ones. First, T_c is much lower, by a factor of 2–5. Also, static antiferromagnetism (AF) extends to much higher doping, so that muon resonance¹ measurements clearly show a Néel temperature T_N *above* the superconducting (SC) T_c in underdoped NCCO, $\text{Nd}_{2-x}\text{Ce}_x\text{CuO}_4$ for $x < 0.15$. At optimal doping, $x = 0.15$, on which we concentrate in the following, the static AF response abruptly disappears, but another signal, indicating AF correlations without long-range order, persists for $T < T_c$.^{1,2} In contrast, the *p*-doped compounds have a wide “pseudogap” region in the phase diagram, between the AF and SC phases.^{3,4}

The ARPES “effective band” electron response in the two classes of compounds also appears to be quite different. In BSCCO and YBCO, the SC ARPES profile at the van Hove (vH, antinodal) point is dominated by the so-called peak-dip-hump structure.^{5,6,7} There is a clear gap of the order of several T_c , the “leading-edge scale,” which tapers to zero at the nodal point in optimally doped (OP) BSCCO, but persists in the slightly underdoped case, albeit without the narrow peak. In NCCO, a wide structure disperses quickly across the Fermi level at both nodal and antinodal points. A visible pseudogap persists only at the “hot spot” for AF scattering, where the ARPES intensity drops sharply as the Fermi surface crosses the skew-diagonal of the zone.^{8,9,10,11,12,13} This is a precursor of the AF gap, which opens on the skew-diagonal for $T < T_N$. The Fermi surface surmised from these measurements is hole-like in both BSCCO and NCCO, but with a different shape, a rounded square around the (π, π) point for BSCCO, and nearly a circle for NCCO.

These results are discussed here within the three band Hubbard model (Emery model),^{14,15} which treats the *p*- and *n*-doped planar CuO_2 cuprates on equal footing from the outset. It introduces the difference Δ_{pd} between the

O and Cu site energies, and the Cu–O and O–O hoppings, t_{pd} and t_{pp} respectively, together with the large interaction U_d between the two holes on the Cu site. These parameters reflect the chemistry of the CuO_2 planes and are therefore expected to be similar for a given material upon both *p* ($\delta > 0$) and *n* ($\delta < 0$) dopings. The physical regime which appears to be appropriate for high- T_c SC corresponds^{16,17} to $\Delta_{pd} > |t_{pd}| > |t_{pp}|$, with $|t_{pp}|$ and t_{pd}^2/Δ_{pd} of the same order of magnitude. The AF order is suppressed asymmetrically, typically for $\delta > 0.01$ on the *p* side and $-\delta > 0.1$ on the *n* side.

An alternative approach often applied to NCCO is the one-band Hubbard model, viewed “from the insulator.”^{18,19,20} It attempts to face experiment by taking into account the oxygen degree of freedom at least through a large $t' \cos k_x \cos k_y$ term, a contribution of the same symmetry as direct O–O hopping.¹⁶ Models with more than three bands are also sometimes considered,²¹ while on the *p*-doped side three-band approaches have been used to discuss (stripe) inhomogeneities.^{22,23}

In the Emery model, the asymmetry of AF and other physical properties between the *p*- and *n*-dopings comes from the different role of U_d in the two cases. It is conveniently observed in the mean-field (MF) slave-boson (SB) approximation for $U_d \rightarrow \infty$, which replaces the “bare” chemical parameters Δ_{pd} and t_{pd} with their renormalized values Δ_{pf} and t , respectively, with t_{pp} unchanged, in an effective free three-band model, with a definite dependence of the renormalized parameters on both the chemical ones and on δ . Although crude, the MF, paramagnetic, translationally invariant version of this theory, combined with harmonic fluctuations of the SB field around the MF saddle point, gives^{16,24} physically reasonable band structures in the metallic regime.²²

The possible three-band regimes in the Emery model in such a situation have been extensively classified.¹⁶ In the presence of the unrenormalized direct oxygen-oxygen hopping t_{pp} , the signature of strong renormalization is a regime change,²⁵ from $0 < -t_{pp} < t_{pd}, \Delta_{pd}/4$ to $-t_{pp} > t, \Delta_{pf}/4 > 0$. In particular, $\Delta_{pf} < 4|t_{pp}|$ means

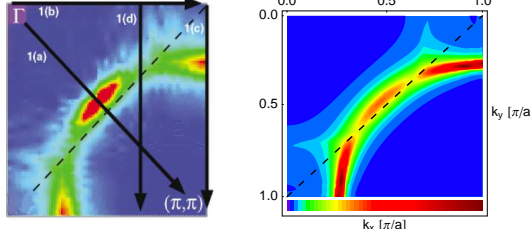


FIG. 1: Left: experimental¹⁰ NCCO ARPES intensity at the Fermi level for $T < 20$ K, $T_c = 24$ K. Right: present calculation.

that the intrinsic band-width of the oxygen band exceeds the effective copper-oxygen splitting, so there occurs an “anticrossing,” in which the lowest (bonding) hole band acquires a significant oxygen character.

Although the main effects of U_d on the overlap t are similar on the p - and n -sides, the renormalization mechanism is different. In the former, paramagnetic charge interactions push the doped holes onto the oxygen sites. This leads to a paramagnetic “resonant band” regime, $\Delta_{pf} \approx 4|t_{pp}|$, useful in BSCCO.²⁴ In NCCO, doping puts carriers on the copper sites. Long-range AF survives to large n -dopings, but at some point there are enough carriers for a significant gain in kinetic energy, if they could spend more time on the oxygens. This is expressed by a band renormalization into the anticrossing regime, $-4t_{pp} \gg \Delta_{pf} > 0$, which thus corresponds to a paramagnetic “lower Hubbard band.”

The correlations omitted by the MF approach can also be described in terms of the same bare parameters. In this scheme, far enough from the AF transition, the magnetic correlations can be treated as dispersive paramagnons, and included in a one-loop calculation:²⁴

$$\Sigma_R(\mathbf{k}, \omega) \propto -F \int d^2q \int_{-\infty}^{\infty} d\omega' \left[\chi_R(\mathbf{Q} + \mathbf{q}, \omega - \omega') (1 - f(\omega')) \text{Im} G_R^{(0)}(\mathbf{k} - \mathbf{q} - \mathbf{Q}, \omega') + G_R^{(0)}(\mathbf{k} - \mathbf{q} - \mathbf{Q}, \omega - \omega') n(\omega') \text{Im} \chi_R(\mathbf{Q} + \mathbf{q}, \omega') \right], \quad (1)$$

where F is an effective interaction constant and $\mathbf{Q} = (\pi, \pi)$. The first term is the magnon propagator convoluted with the electron response, the second, vice versa. Both are equally important in BSCCO, but the one with the boson occupation number dominates in NCCO.

In Figure 1 we compare our results with experiment. The Fermi surface is first fitted to obtain the renormalized parameters of the three-band model. We can easily reproduce the shape of the Fermi surface in NCCO in a regime very similar to the one in BSCCO,²⁴ namely with $\Delta_{pf} > -t_{pp} \gg t > 0$, the main difference being that Δ_{pf} is now smaller than in BSCCO: $\Delta_{pf} = 1.6$ eV,

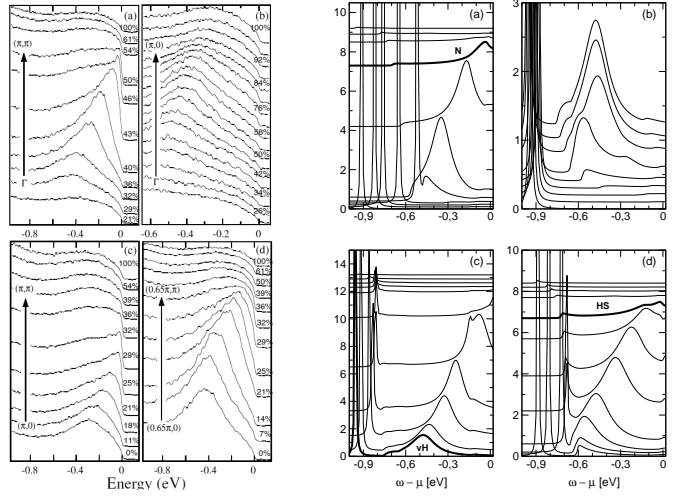


FIG. 2: Left: experimental¹⁰ ARPES profiles for the cuts (a)–(d) in Fig. 1. The positions in the zone are indicated as percentages along the ranges given by arrows. Right: calculated ARPES profiles for the same positions, without the Fermi factor. The nodal $(\pi/2, \pi/2)$, van Hove $(\pi, 0)$, and hot-spot $(0.65\pi, 0.36\pi)$ profiles are indicated with heavy lines.

$t_{pp} = -1.2$ eV and $t = 0.3$ eV, deep in the anticrossing regime. It is noteworthy that the zeroth-order band prediction indicates that the effect of the oxygen hopping t_{pp} is as large in the n -doped cuprates as in the p -doped ones. The Fermi surface in Fig. 1 is actually found beyond the anticrossing point of the bonding dispersion, where the wave-functions have significant oxygen character, making the argument in favor of anti-crossing self-consistent. This regime cannot be reached consistently from the single-band Hubbard model.

The paramagnon fit parameters are: band-edge $\tilde{\omega} = 0.001$ eV $< kT = 0.002$ eV $< \gamma = 0.004$ eV (damping), cutoff $\omega_0 = 0.15$ eV, coupling constant $F = 0.77$ eV, giving a self-energy range shown in Fig. 3 below. The main input scales are all taken from experiment.^{1,10} The calculation is not sensitive to the magnon damping and cutoff, kept roughly similar as in BSCCO. The only free parameter left is the coupling constant F . With this one adjustment, all ARPES scales, dispersions and widths in Fig. 2 were obtained rather well. Even smaller experimental features have their counterparts in theory, such as the flattening of the peak on the $(\pi, 0)$ – (π, π) line, discussed below, and the difference in dispersion shape (trend of the peaks) between panels (c) and (d) in Fig. 2.

The chemical potential (relative to the vH point) in this fit, $\mu = 0.75$ eV, is more than twice as large than experiment seems to suggest. The experimental panel (c) in Fig. 2 shows that the ARPES profile at the vH point has a maximum at about 0.35 eV binding energy. The lowest curve in the theoretical panel (c) in the same figure explains the discrepancy: the “bump” there is in fact the upper wing of a spectral intensity split by AF interactions. In this way the apparent Fermi level mismatch

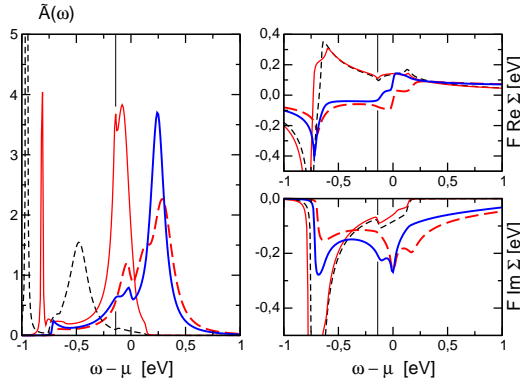


FIG. 3: Spectral intensities and the corresponding self-energies at selected points in the Brillouin zone. Thin dashed line: vH point. Thin full line: 25% of the zone away from it in the direction of the AF point. Thick full line: hot spot. Thick dashed line: 50% of the zone in the nodal direction $k_x = k_y$. The transition to the pseudogapped regime around E_F is emphasized by drop-down thin lines at $\omega - \mu = -0.14$ eV.

is resolved, without spoiling the zeroth-order Fermi surface fit, as evident from Fig. 1. The narrow lower wing at nearly 1 eV binding corresponds to the experimental ARPES intensity rising again at higher energy. In the approach from the paramagnetic metal, high-energy features are subject to further corrections, so let us first focus on the wide dispersive upper wings.

Our calculation in Fig. 2 gives the impression that all the wide features observed in OP NCCO are incoherent. Experimentally,¹⁰ in addition to the hot spot, there is also a drop in intensity in the nodal direction *before* the Fermi level is approached. This is exactly the opposite behavior than one would expect from a quasiparticle. To emphasize the point, theoretical curves are shown without the Fermi factor, and it is clear that the same phenomenon is occurring in the calculation as well. We extend the experimental observation,¹⁰ and claim that the Fermi surface in OP NCCO is pseudogapped everywhere.

A detailed analysis is given in Figure 3. At the vH point, the chemical potential puts a quasiparticle at 0.75 eV binding energy, but the self-energy shows that this is in the middle of a forbidden region: $\text{Re } \Sigma$ is rising, $\text{Im } \Sigma$ is large around there. The quasiparticle is split, and the wide structure at 0.45 eV appears as the upper part of a split quasiparticle, not necessarily incoherent. As k_y increases along the $(\pi, 0) - (\pi, \pi)$ line, this signal enters another forbidden region, at about ± 0.1 eV around E_F . We have purposefully put a rather low boson damping in the calculation, to observe the moment of transition as a fine structure in the profile at $k_y = 0.25\pi/a$: the small sharp spike is at the edge of the quasiparticle region, while the peak at right is already incoherent. (The experimental profiles at 25% and 29% of the zone in panel (c) of Fig. 2 show a similar flattening at the top.) Loss of coherence as the Fermi energy is approached indicates a pseudogap regime, validating the initial impression.

A similar phenomenon occurs in the nodal direction. The dominant feature is loss of intensity rather than loss of coherence, because the Fermi surface is nearly nested. The quasiparticle loses intensity before entering the pseudogap region around E_F , and reappears at the other side, without really crossing E_F . Succinctly, the antinodal region is pseudogapped because an incoherent signal crosses the Fermi level, while the nodal one is pseudogapped because a coherent signal does not cross it. Technically, $\text{Re } \Sigma$ increases everywhere at the Fermi level, precluding a quasiparticle, while $\text{Im } \Sigma$ is large at the nodal Fermi crossing, because of nesting, but fairly small at the antinodal crossing, which is not nested.

At the hot spot, both effects combine: an incoherent structure is suppressed in intensity before it can cross the Fermi level. Finally, as one moves from the vH point to the Γ -point, the increase in binding energy is accompanied with a loss of both coherence and intensity, as the upper wing of the split quasiparticle approaches the forbidden region below ~ 0.5 eV binding, where the slope $\text{Re } \Sigma$ is positive, and $\text{Im } \Sigma$ is large (see panel (b) of Fig. 2).

The present work establishes a number of parallels and distinctions between BSCCO and NCCO. The chemical potential, relative to the vH point, and the paramagnon coupling constant are much larger in NCCO, the first by a factor of ~ 30 , the second ~ 5 . This makes the main ARPES scales in NCCO significantly larger, ~ 0.5 *vs.* ~ 0.1 eV in BSCCO. The larger coupling constant is a plausible consequence of doping on the coppers, where the carriers enter an otherwise strongly AF-polarized environment, as evident from the wider extension of AF on the *n*-doped side. On the other hand, when enough carriers are doped on the oxygens, the superexchange is only indirectly involved in their magnetic correlations.

The paramagnon physical regime turns out to be significantly different in the two pseudogaps. In SC BSCCO, paramagnons are quantum fluctuations, whose energy scale (41 meV) is much higher than T_c . To put NCCO in the same regime requires a paramagnon band-edge $\tilde{\omega} \sim 10$ meV. We find this at odds with the distinct hot spot in experiment. If the band-edge is comparable with the temperature, and especially if it is lower as here, the hot spot becomes clearly discerned.²⁶ We conclude the paramagnons in SC NCCO are semiclassical, or transitional (the results are similar if $\tilde{\omega} \sim T_c$). Paramagnons in the vicinity of the AF state indeed have low energies.¹

Conversely, if the paramagnon band-edge is lowered in BSCCO, the narrow “antiadiabatic”²⁴ peak near the vH point disappears. This is observed in underdoped BSCCO, as expected if the AF transition is approached. We have argued²⁴ that the low-energy peak only obscures the pseudogap in OP BSCCO, because it is part of the pseudogap profile, not a true quasiparticle. Without it, there remains the usual splitting of the spectral intensity in two peaks, due to AF scattering. In BSCCO, the splitting straddles the Fermi level, and the lower (occupied) wing is sufficiently close to E_F at the $(\pi, 0) - (\pi, \pi)$ line to be incoherent. In NCCO, the chemical potential places

both wings below the Fermi energy at the vH point, and the upper one becomes incoherent as it disperses towards E_F along the same line. Hence the wide dispersive wing in NCCO is analogous to the hump in BSCCO.

Paramagnon damping was a critical parameter in BSCCO, where a switch from over- to underdamped produced the change in ARPES profile observed at T_c .²⁴ By contrast, the parametrization used here for NCCO is only weakly sensitive to the damping regime, which neatly parallels the experimental situation: the changes in ARPES profiles as NCCO becomes superconducting are very slight.^{8,10} This strengthens our assertion²⁴ that SC has also an indirect effect on the ARPES spectra, by gapping out the magnon damping.

In both the BSCCO and NCCO calculations, the region of about ± 150 meV around E_F does not support a quasiparticle, a scale set by the AF interaction. Other sources of decoherence are absent in the numerics, coupling to Mott charge fluctuations and to stripes.²⁷ Both are a natural next step in the present framework.²⁴ Thus Mott fluctuations are expected to account for the rise in response below 0.5 eV binding, found in experiment, by broadening the narrow deeply bound peaks visible in the calculation of Fig. 2. A similar role of Mott fluctuations at the Δ_{pf} scale has been found in the extended Raman background, in the non-crossing approximation.²⁸

We expect our predictions to remain robust at less than 0.5 eV binding. The lowest-energy feature is the coherent-incoherent crossover at ~ 0.15 eV, still high above the SC scale. Neither high-energy (Mott) perturbations, operating at 1–2 eV, nor low-energy (SC) effects

should significantly change the picture given here in the energy window from T_c to ~ 0.5 eV. The precise position of the crossover at 0.15 eV is parameter-dependent, but its existence is not.

The intermediate-energy (~ 0.1 eV) features of ARPES spectra in both BSCCO²⁴ and NCCO, down to the leading-edge scale at the antinodal point in BSCCO, are reproduced by accounting for AF fluctuations alone. If superconductivity, of whatever origin, is simply making use of the available density of states, as calculated here, it obviously follows that T_c should be much higher in BSCCO than in NCCO. This indicates a somewhat more complex structure of the SC gap than a single d -wave, not simply related to the order parameter symmetry.

To conclude, we have accounted for ARPES spectra in NCCO focussing exclusively on dispersive paramagnons, without low-energy magnetic responses, in the same simple approach²⁴ as previously for BSCCO. We explain the observed differences by a change in the physical regime of the paramagnons, semiclassical in NCCO as opposed to quantum in BSCCO, and a much larger value of the effective coupling constant. Both are consistent with the vicinity of the AF transition in NCCO. Optimally doped NCCO is pseudogapped on the whole Fermi surface, and the wide dispersive features are analogous to the hump in BSCCO. Direct oxygen-oxygen hopping is as important in NCCO as in BSCCO. The phenomenological value of the Cu–O hopping in NCCO indicates, as expected, that it is renormalized by the strong on-site repulsion.

This work was supported by the Croatian Government under Project 0119256.

* Electronic address: dks@phy.hr

† Electronic address: sbarisić@phy.hr

¹ T. Uefuji et al., *Physica C* **357-60**, 208 (2001).

² K. Yamada et al., *J. Phys. Chem. Solids* **60**, 1025 (1999).

³ H. Ding et al., *Nature* **382**, 51 (1996).

⁴ A. G. Loeser et al., *Science* **273**, 325 (1996).

⁵ J. C. Campuzano et al., *Phys. Rev. Lett.* **83**, 3709 (1999).

⁶ A. V. Fedorov et al., *Phys. Rev. Lett.* **82**, 2179 (1999).

⁷ D. H. Lu et al., *Phys. Rev. Lett.* **86**, 4370 (2001).

⁸ N. P. Armitage et al., *Phys. Rev. Lett.* **86**, 1126 (2001).

⁹ Y. Onose et al., *Phys. Rev. Lett.* **87**, 217001 (2001).

¹⁰ N. P. Armitage et al., *Phys. Rev. Lett.* **87**, 147003 (2001).

¹¹ T. Sato et al., *Science* **291**, 1517 (2001).

¹² N. P. Armitage et al., *Phys. Rev. Lett.* **88**, 257001 (2002).

¹³ G. Blumberg et al., *Phys. Rev. Lett.* **88**, 107002 (2002).

¹⁴ V. J. Emery, *Phys. Rev. Lett.* **58**, 2794 (1987).

¹⁵ C. M. Varma et al., *Solid State Commun.* **62**, 681 (1987).

¹⁶ I. Mrkonjić and S. Barišić, *Eur. Phys. J. B* **34**, 69 (2003).

¹⁷ I. Mrkonjić and S. Barišić, *Eur. Phys. J. B* **34**, 441 (2003).

¹⁸ K. Kuroki et al., *J. Low Temp. Phys.* **117**, 247 (1999).

¹⁹ C. Kusko et al., *Phys. Rev. B* **66**, 140513(R) (2002).

²⁰ B. Kyung et al., *Phys. Rev. Lett.* **93**, 147004 (2004).

²¹ A. Bansil et al., *New J. Phys.* **7**, 140 (2005).

²² J. Lorenzana and G. Seibold, *Phys. Rev. Lett.* **89**, 136401 (2002).

²³ P. Abbamonte et al., *Nature Physics* **1**, 155 (2005).

²⁴ D. K. Sunko and S. Barišić, *Eur. Phys. J. B* **46**, 269 (2005).

²⁵ I. Mrkonjić and S. Barišić, *Phys. Rev. Lett.* **92**, 129701 (2004).

²⁶ D. K. Sunko and S. Barišić, in *Proc. SPIE, Strongly Correlated Electron Materials: Physics and Nanoengineering*, edited by I. Bozovic and D. Pavuna (SPIE, 2005), vol. 5932, pp. 71–83.

²⁷ S. A. Kivelson et al., *Rev. Mod. Phys.* **75**, 1201 (2003).

²⁸ H. Nikšić et al., *Physica C* **241**, 247 (1995).